Electronic Supplementary Material (ESI) for Chemical Science.

Supporting information for

Oxygen Chemisorption/Desorption in a Reversible Single-Crystal-To-Single-Crystal Transformation

Jonas Sundberg,[a] Lisa Cameron,[b] Peter Southon,[b] Cameron J. Kepert[b] and Christine J. McKenzie*[a]

[a] Department of Physics, Chemistry and Pharmacy, University of Southern Denmark, Campusvej 55, 5230 Odense M, Denmark; [b] School of Chemistry, The University of Sydney, NSW 2006.

E-mail: mckenzie@sdu.dk

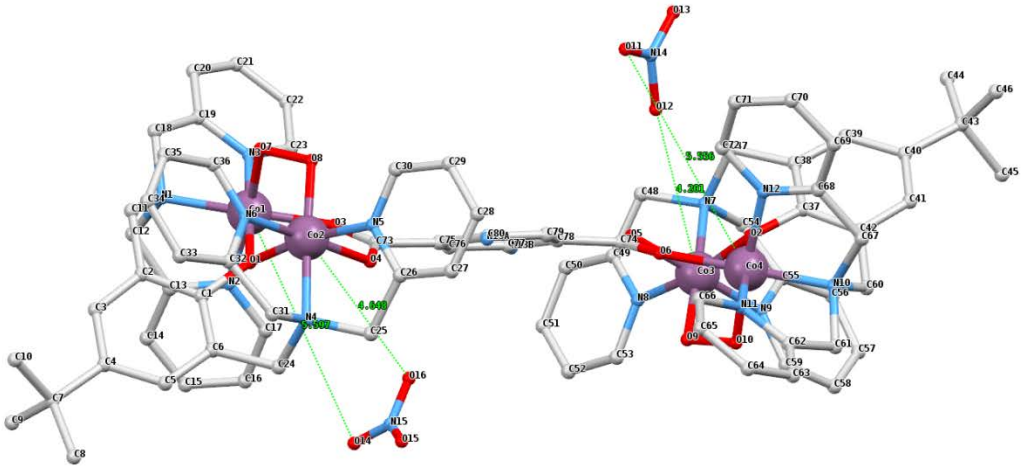

Figure S1(a). Nitrate counteranions closest to the dicobalt sites

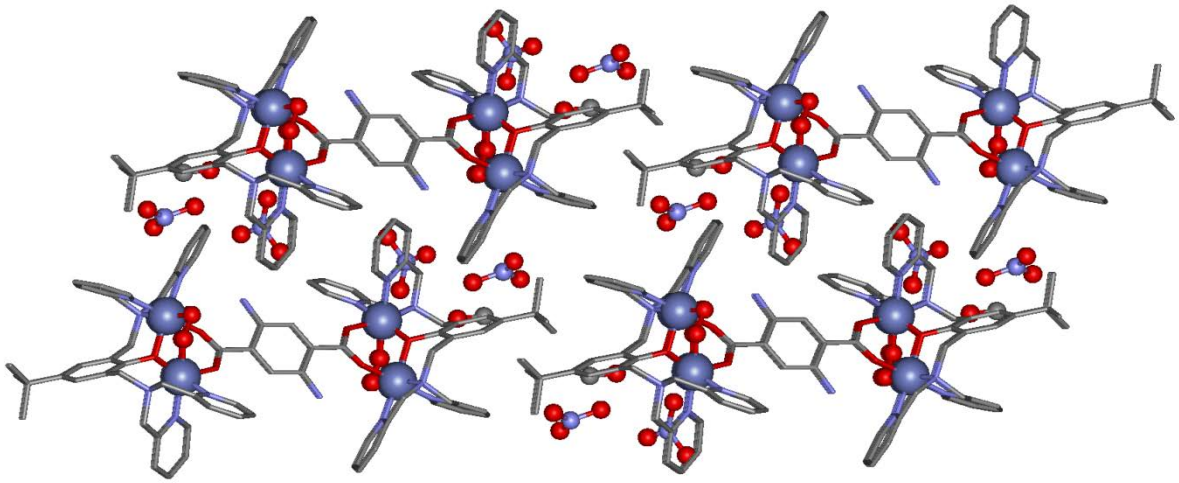

Figure S1(b) Illustration of oxygenated structure, viewed down the *b* axis. Selected atoms are shown as balls to illustrate aspects of the structure (Co = large blue balls, N = small blue balls, O = red balls). Carbon atoms are shown as vertices, while hydrogen atoms and solvent molecules are omitted for clarity.

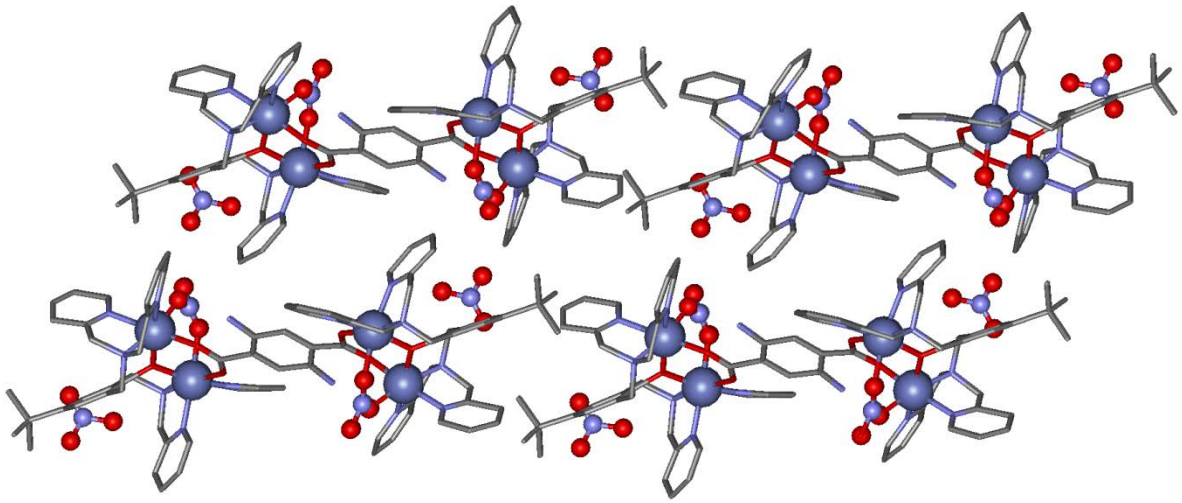

Figure S1(c) Illustration of deoxygenated structure, viewed down the *b* axis. Selected atoms are shown as balls to illustrate aspects of the structure (Co = large blue balls, N = small blue balls, O = red balls). Carbon atoms are shown as vertices, while hydrogen atoms and solvent molecules are omitted for clarity.

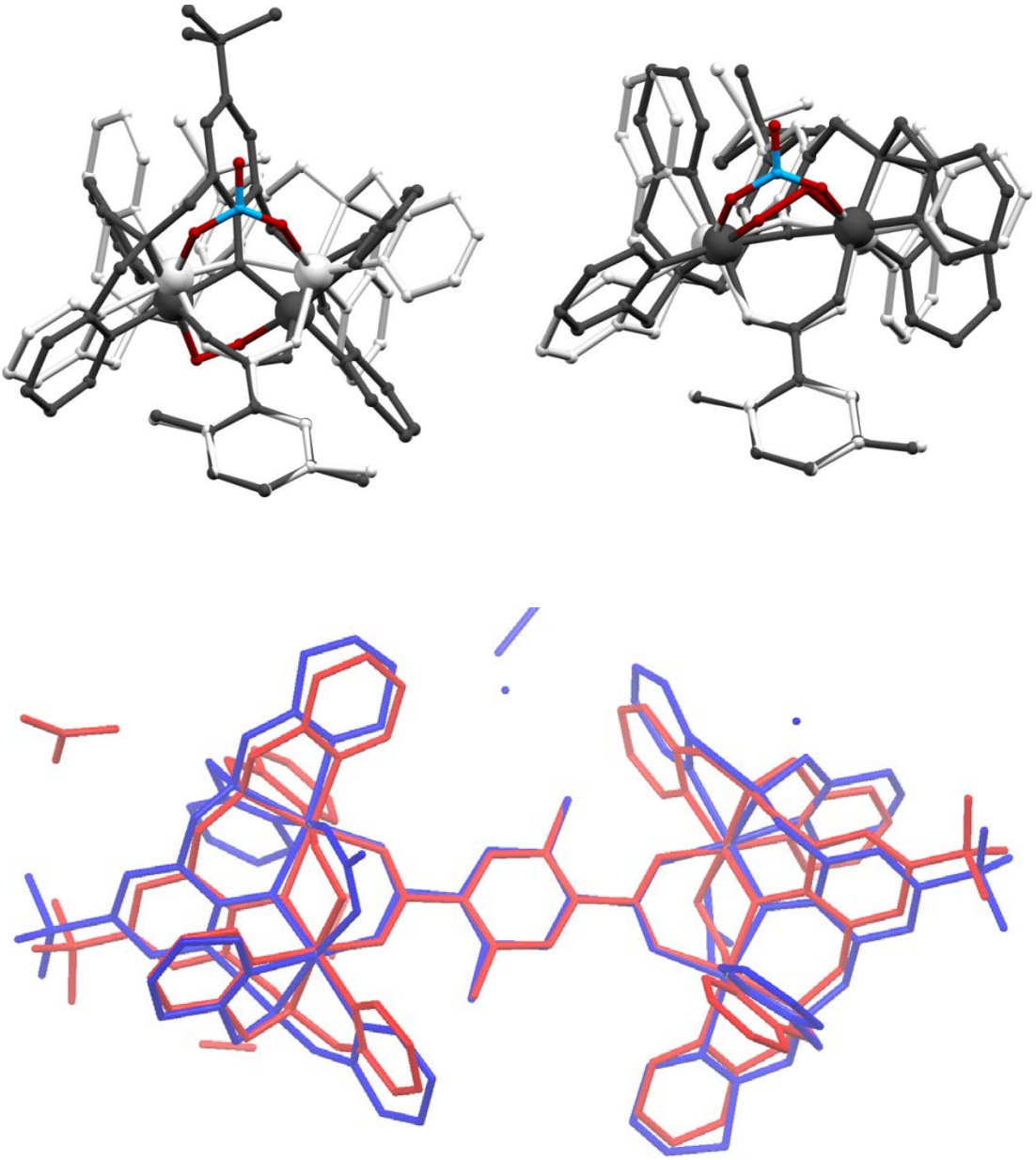

Figure S2. **(a)** Comparison of the geometrical arrangement of $bpbp^-$ in the oxy- and deoxy-form of **2b**$(NO_4)_4$ when O_2^{2-} and NO_3^- are bonded to Co_2-unit on the same or opposite plane. **(b)** Overlay of the [{(bpbp)Co_2}$_2$(NH_2bdc)] unit for the oxygenated (red) and deoxygenated (blue) structures, showing distortions in the unit with removal of oxygen and binding of nitrate anion.

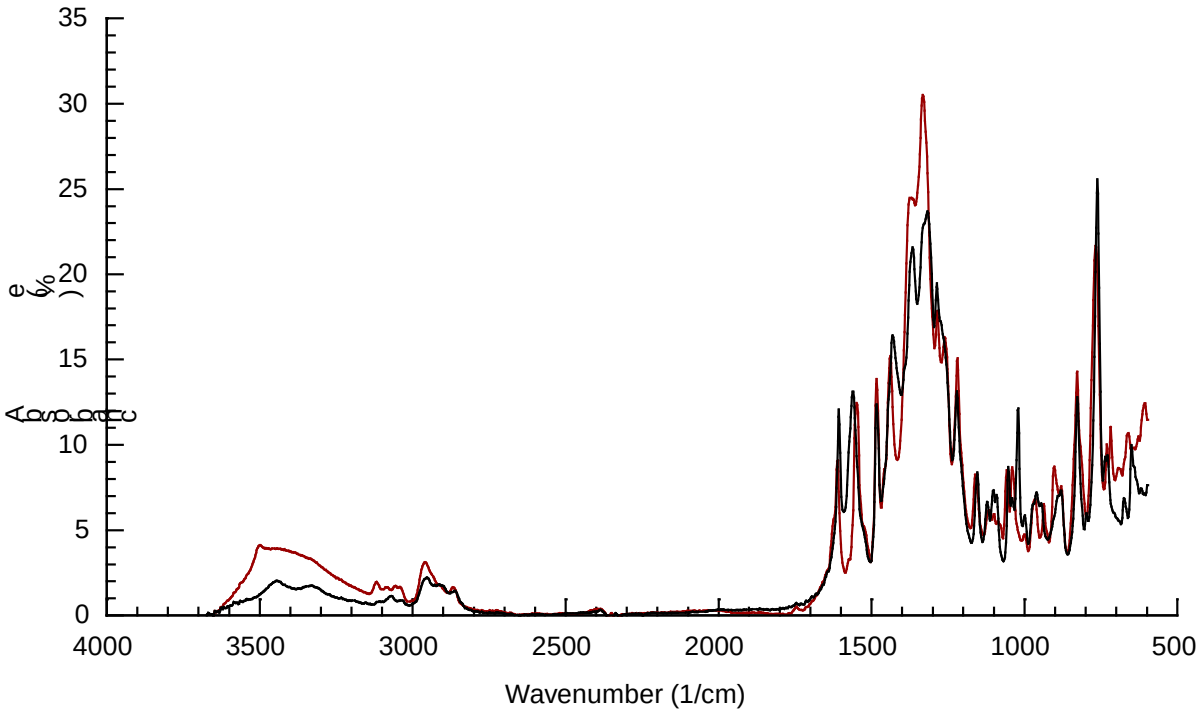

Figure S3. IR spectra of **2b**$(NO_4)_4$•$7H_2O$ at -20 °C (red) and 120 °C (black) showing reduction in intensity of the broad band at 3000 to 3500 cm^{-1} attributed to loss of water.

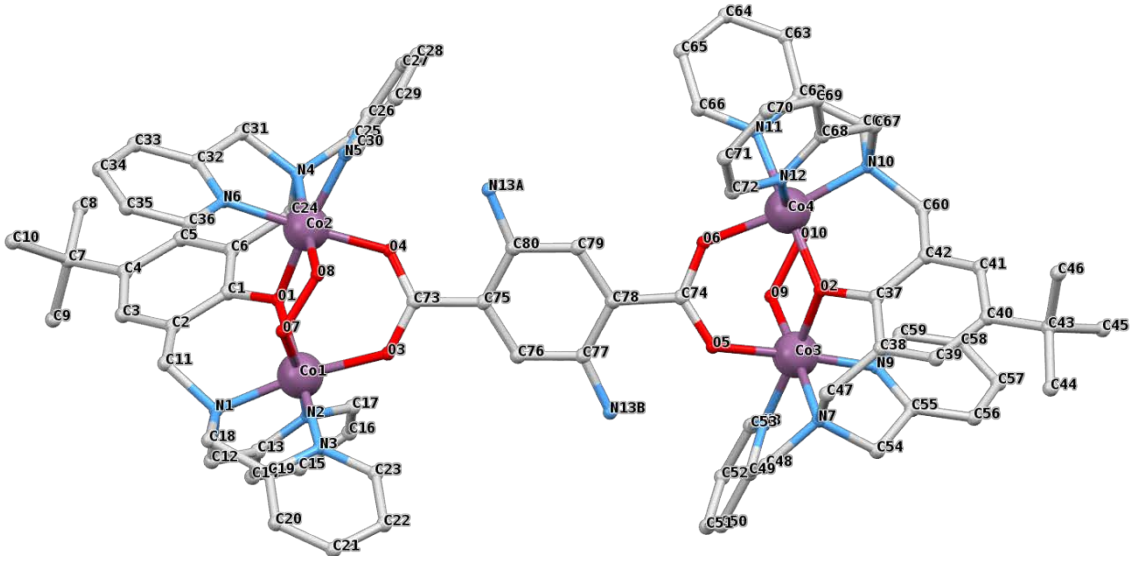

Figure S4. Molecular structure with atom numbering scheme of the cation in $[\{(bpbp)Co_2(O_2)\}_2(NH_2bdc)](NO_3)_4 \cdot 7H_2O$.

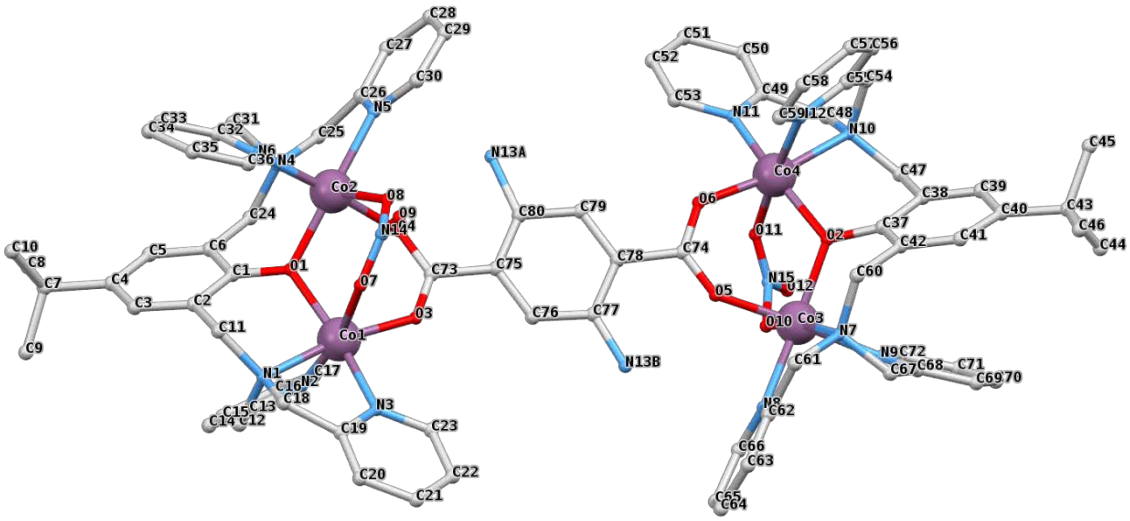

Figure S5. Molecular structure with atom numbering scheme of the cation in $[\{(bpbp)Co_2(NO_3)\}_2(NH_2bdc)](NO_3)_2 \cdot 2H_2O$.

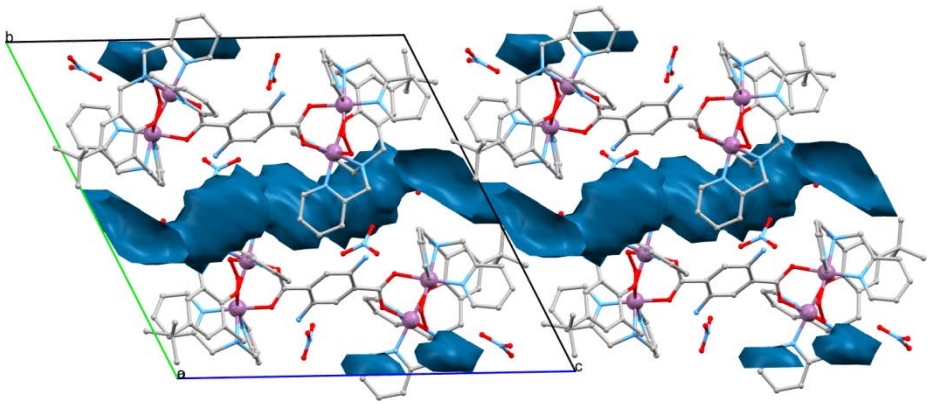

Figure S6. View of **2b**$(NO_3)_4$ (lattice water removed *in silico*) down the *a*-axis showing voids running parallel to the *b*-axis. Void calculation was performed in Mercury CSD 3.3.1 with a probe radius of 1.2Å and grid spacing 0.7Å resulting in a volume of 200.18 $Å^3$ / 4.8% per unit cell

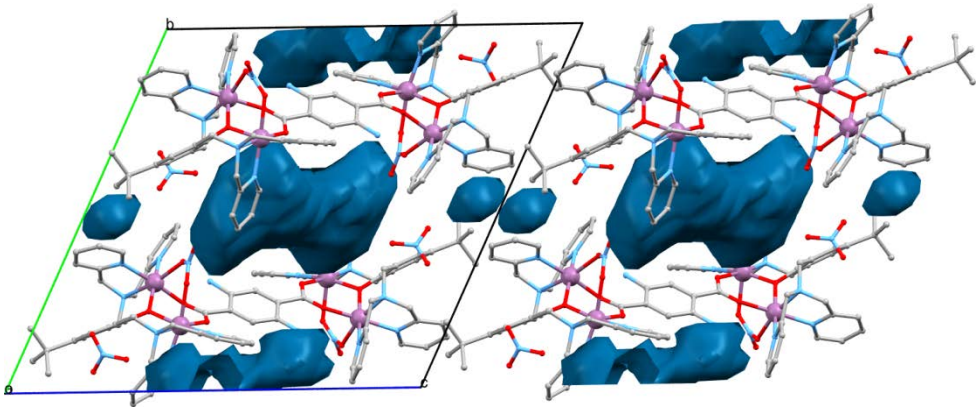

Figure S7. View of **2b**$_{\mathbf{deoxy}}(NO_3)_4$ (lattice water removed *in silico*) down the *a*-axis showing how the voids running parallel to the *b*-axis become disconnected. Void calculation was performed in Mercury CSD 3.3.1 with a probe radius of 1.2Å and grid spacing 0.7Å resulting in a volume of 300.99 $Å^3$ / 7.0% per unit cell

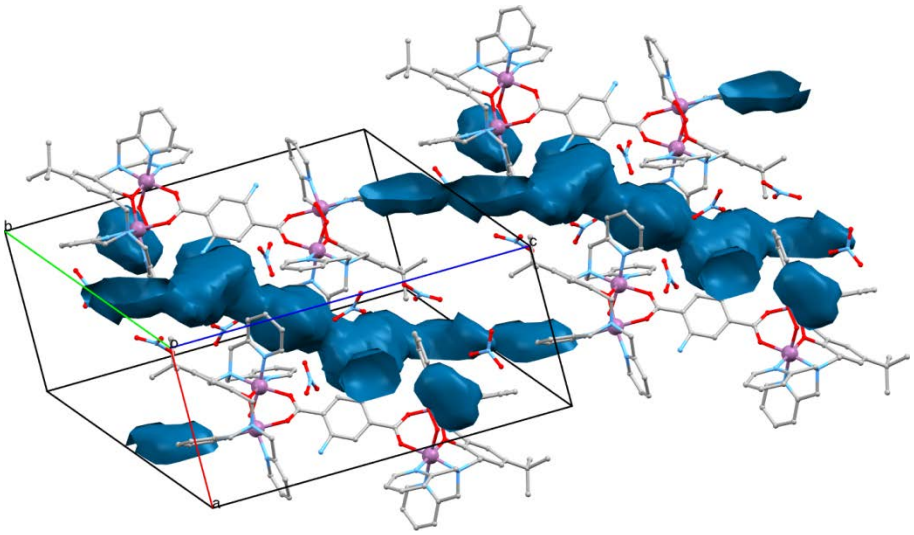

Figure S8. Perspective view the voids in of **2b**$(NO_3)_4$ (lattice water removed *in silico*).

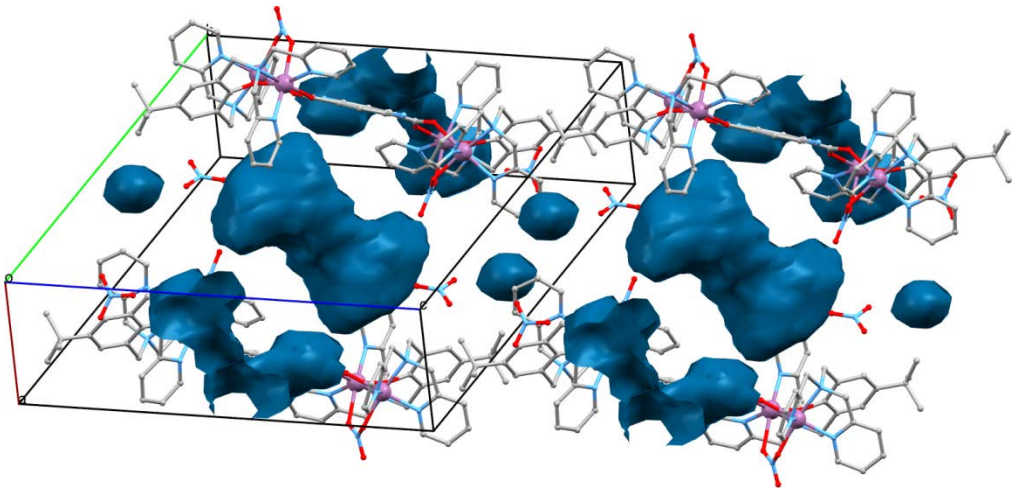

Figure S9. Perspective view the voids in of **2b$_{deoxy}$**$(NO_3)_4$ (lattice water removed *in silico*).

Table S1. Selected bond distances (Å) and angles (°).

	$[\{(bpbp)Co_2(O_2)\}_2(NH_2bdc)](NO_3)_4\cdot 7H_2O$	$[\{(bpbp)Co_2(NO_3)\}_2(NH_2bdc)](NO_3)_2\cdot 2H_2O$
Co1 - O1	1.895(6)	1.996(5)
Co1 - O3	1.934(6)	1.990(5)
Co1 - O7 (**O_2**)	2.011(5)	-
Co1 - O7 (**NO_3**)	-	2.271(6)
Co1 - N1	1.961(8)	2.174(6)
Co1 - N2	1.976(8)	2.098(7)
Co1 - N3	1.910(8)	2.129(7)
Co2 - O1	1.894(7)	2.011(5)
Co2 - O4	1.904(6)	2.106(5)
Co2 - O8 (**O_2**)	1.879(7)	-
Co2 – O8 (**NO_3**)	-	2.100(6)
Co2 - N4	2.013(8)	2.135(7)
Co2 - N5	1.911(9)	2.141(7)
Co2 - N6	1.917(8)	2.131(7)
Co3 - O2	1.896(6)	2.011(5)
Co3 - O5	1.927(6)	2.071(5)
Co3 - O9 (**O_2**)	1.868(6)	-
Co3 - O10 (**NO_3**)	-	2.100(7)
Co3 - N7	2.012(7)	2.151(7)
Co3 - N8	1.899(7)	2.174(7)
Co3 - N9	1.907(8)	2.127(7)
Co4 - O2	1.910(6)	1.982(5)
Co4 - O6	1.936(6)	2.020(7)
Co4 - O10 (**O_2**)	1.866(6)	-
Co4 - O11 (**NO_3**)	-	2.275(9)
Co4 - N10	1.966(8)	2.172(8)
Co4 - N11	1.920(7)	2.043(9)
Co4 - N12	1.981(8)	2.068(7)
Co1 - Co2	3.164(2)	3.424(1)
Co3 - Co4	3.177(2)	3.473(2)
O7 - O8	1.416(9)	-
O9 - O10	1.431(9)	-

Co1 - O1 - Co2	113.2(3)	117.4(2)
Co3 - O2 - Co4	113.1(3)	120.8(2)
N1 - Co1 - O1	95.4(3)	89.8(2)
N1 - Co1 - O3	171.6(3)	169.8(3)
N1 - Co1 - O7	90.0(3)	89.8(2)
N1 - Co1 - N2	84.9(3)	80.9(3)
N1 - Co1 - N3	83.6(3)	76.5(3)
N2 - Co1 - O1	89.6(3)	88.0(2)
N2 - Co1 - O3	91.1(3)	98.6(3)
N2 - Co1 - O7	171.4(3)	168.2(2)
N2 - Co1 - N3	96.1(3)	101.9(3)
N3 - Co1 - O1	174.1(3)	161.4(3)
N3 - Co1 - O3	89.5(3)	93.7(3)
N3 - Co1 - O7	90.1(3)	82.7(3)
O1 - Co1 - O3	92.0(3)	100.3(2)
O1 - Co1 - O7	84.1(3)	84.7(2)
O3 - Co1 - O7	94.8(3)	91.9(2)
N4 - Co2 - O1	92.3(3)	92.5(2)
N4 - Co2 - O4	92.2(3)	96.3(2)
N4 - Co2 - O8	177.2(3)	168.9(2)
N4 - Co2 - N5	81.9(4)	78.0(3)
N4 - Co2 - N6	85.2(3)	80.3(3)
N5 - Co2 - O1	170.1(3)	167.5(3)
N5 - Co2 - O4	83.3(3)	82.4(3)
N5 - Co2 - O8	95.3(4)	92.5(3)

N5 - Co2 - N6	94.5(3)	99.6(3)
N6 - Co2 - O1	93.0(3)	86.6(2)
N6 - Co2 - O4	176.8(3)	175.6(3)
N6 - Co2 - O8	95.5(3)	95.7(3)
O1 - Co2 - O4	89.0(3)	90.7(2)
O1 - Co2 - O8	90.3(3)	97.7(2)
O4 - Co2 - O8	86.9(3)	88.2(2)
N7 - Co3 - O2	91.5(3)	92.0(2)
N7 - Co3 - O5	92.3(3)	98.6(2)
N7 - Co3 - O9 / O10	177.2(3)	168.7(3)
N7 - Co3 - N8	82.7(3)	77.1(3)
N7 - Co3 - N9	86.1(3)	78.9(3)
N8 - Co3 - O2	171.0(3)	166.4(3)
N8 - Co3 - O5	85.5(3)	81.5(2)
N8 - Co3 - O9 / O10	94.7(3)	98.2(3)
N8 - Co3 - N9	91.8(3)	94.6(3)
N9 - Co3 - O2	94.7(3)	91.0(2)
N9 - Co3 - O5	177.0(3)	175.8(3)
N9 - Co3 - O9 / O10	95.0(3)	91.5(3)
O2 - Co3 - O5	87.8(2)	92.4(2)
O2 - Co3 - O9 / O10	91.0(3)	93.9(2)
O5 - Co3 - O9 / O10	86.5(3)	90.7(3)
N10 - Co4 - O2	96.5(3)	89.4(2)
N10 - Co4 - O6	172.0(3)	171.7(3)
N10 - Co4 - O10 / O11	90.3(3)	92.9(4)
N10 - Co4 - N11	83.1(3)	78.9(4)
N10 - Co4 - N12	85.6(3)	80.6(3)
N11 - Co4 - O2	176.8(3)	160.9(4)
N11 - Co4 - O6	89.5(3)	93.7(4)
N11 - Co4 - O10 / O11	92.5(3)	79.9(4)
N11 - Co4 - N12	87.8(3)	98.7(3)
N12 - Co4 - O2	95.3(3)	94.1(2)
N12 - Co4 - O6	90.9(3)	97.1(3)
N12 - Co4 - O10 / O11	175.8(3)	173.5(4)
O2 - Co4 - O6	91.0(3)	98.7(2)
O2 - Co4 - O10 / O11	84.4(3)	85.7(3)
O6 - Co4 - O10 / O11	93.2(3)	89.4(4)

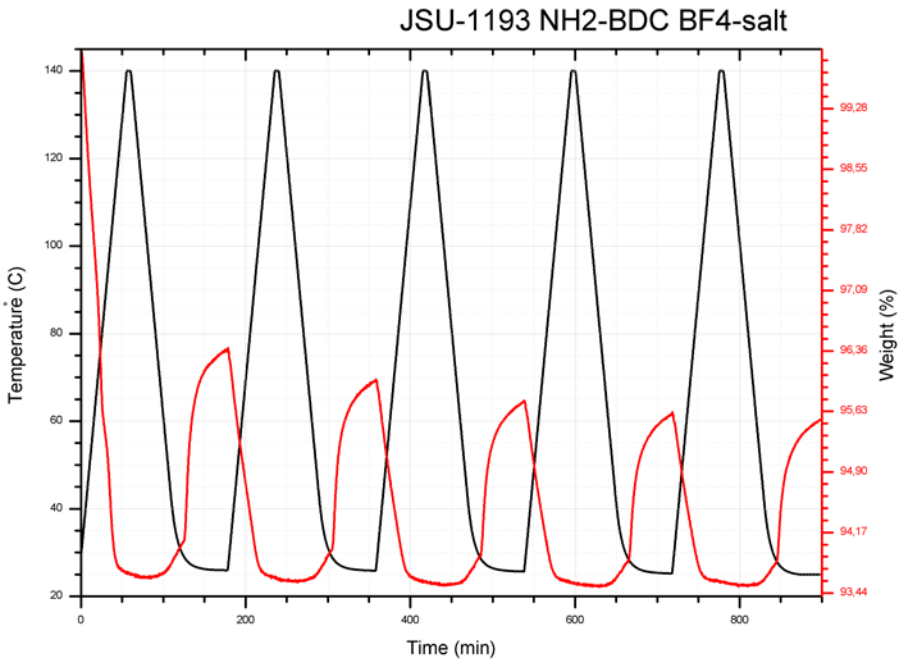

Figure S10. Temperature dependent cycling of reversible O_2 binding by **2b**$(BF_4)_4$ measured using TGA.

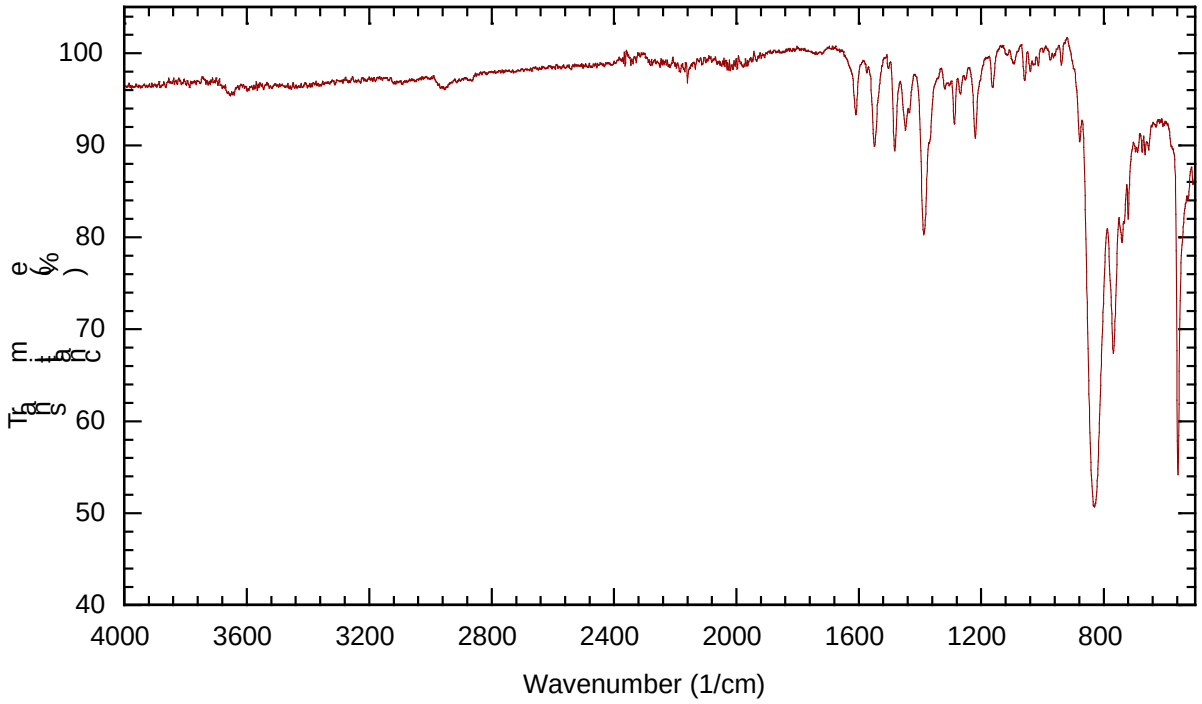

Figure S11. FT-IR Spectra of $[\{Co_2(bpbp)(O_2)\}_2(bdc)](PF_6)_4$.

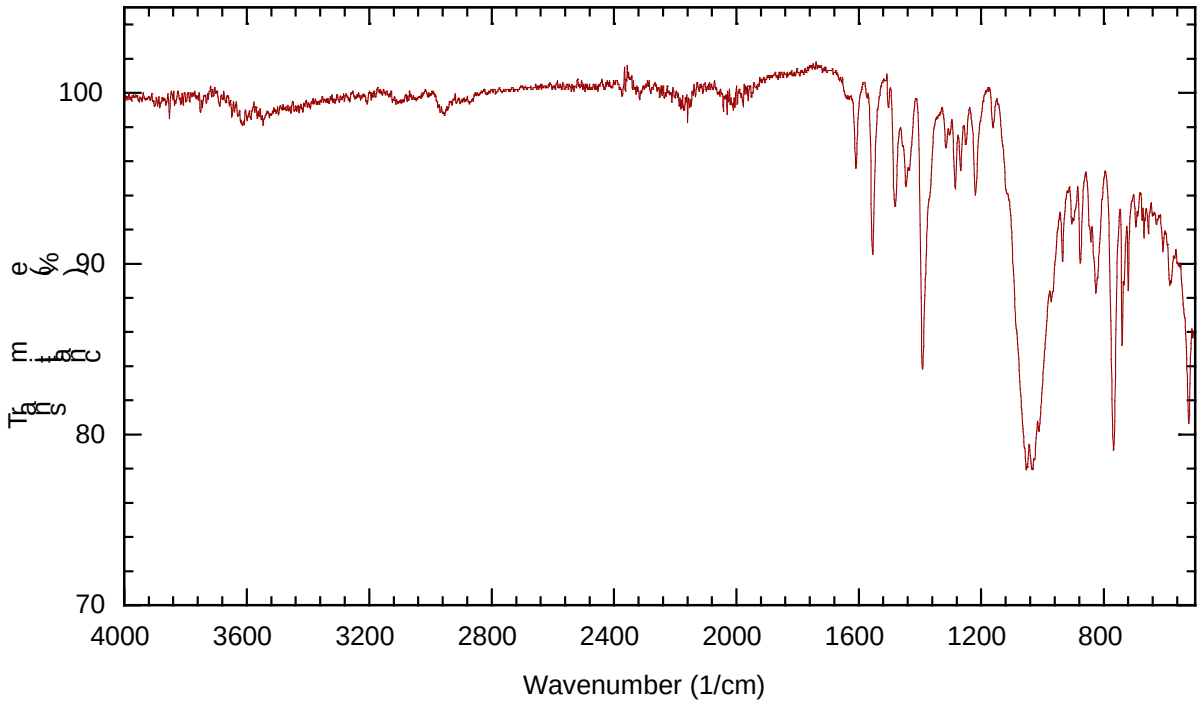

Figure S12. FT-IR Spectra of $[\{Co_2(bpbp)(O_2)\}_2(bdc)](BF_4)_4$.

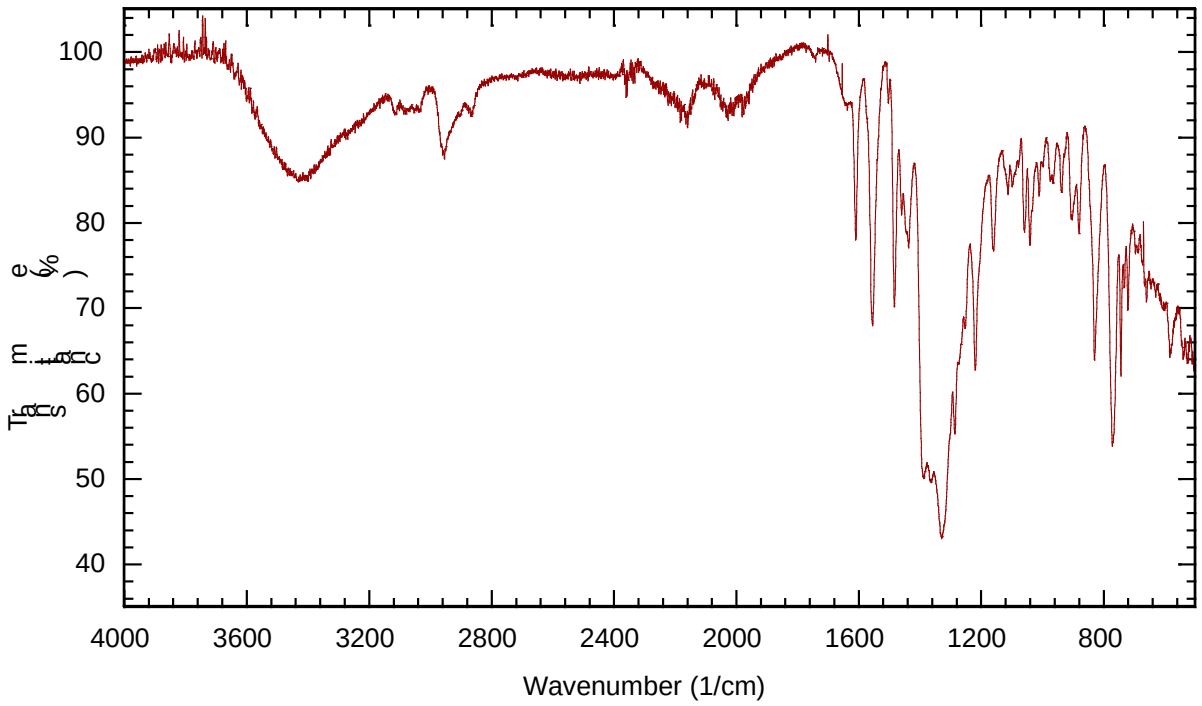

Figure S13. FT-IR Spectra of [{Co_2(bpbp)(O_2)}$_2$(bdc)](NO_3)$_4$.

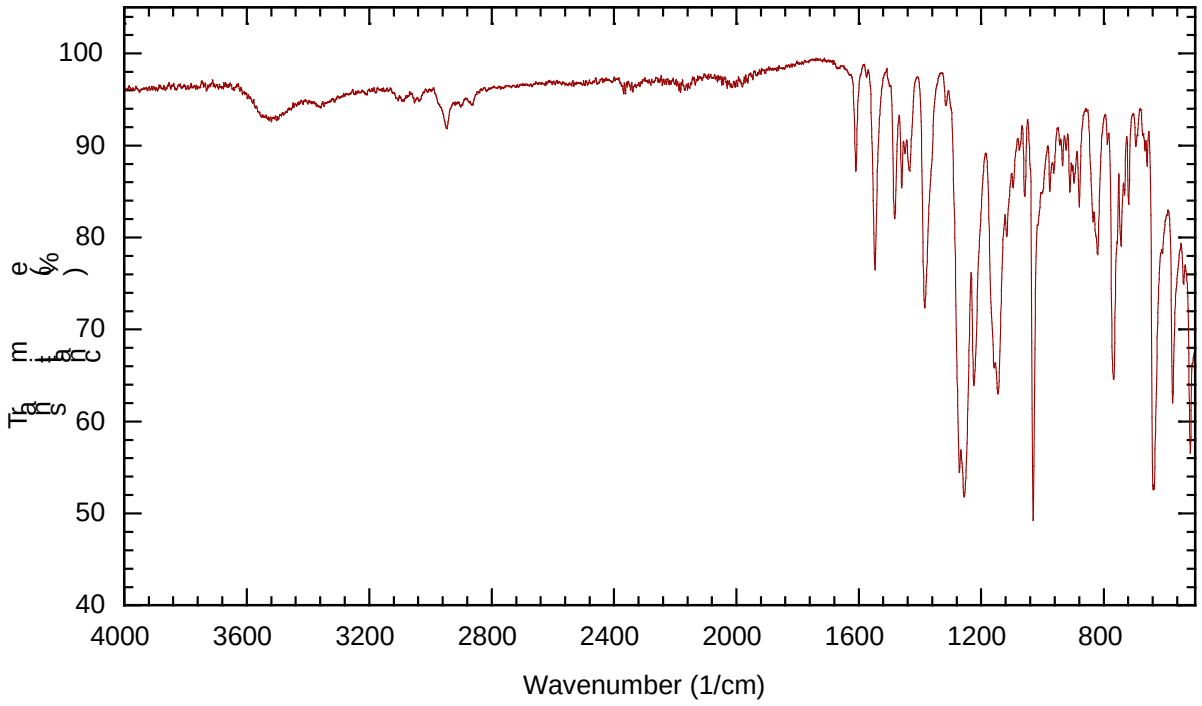

Figure S14. FT-IR Spectra of [{Co_2(bpbp)(O_2)}$_2$(bdc)](OTf)$_4$.

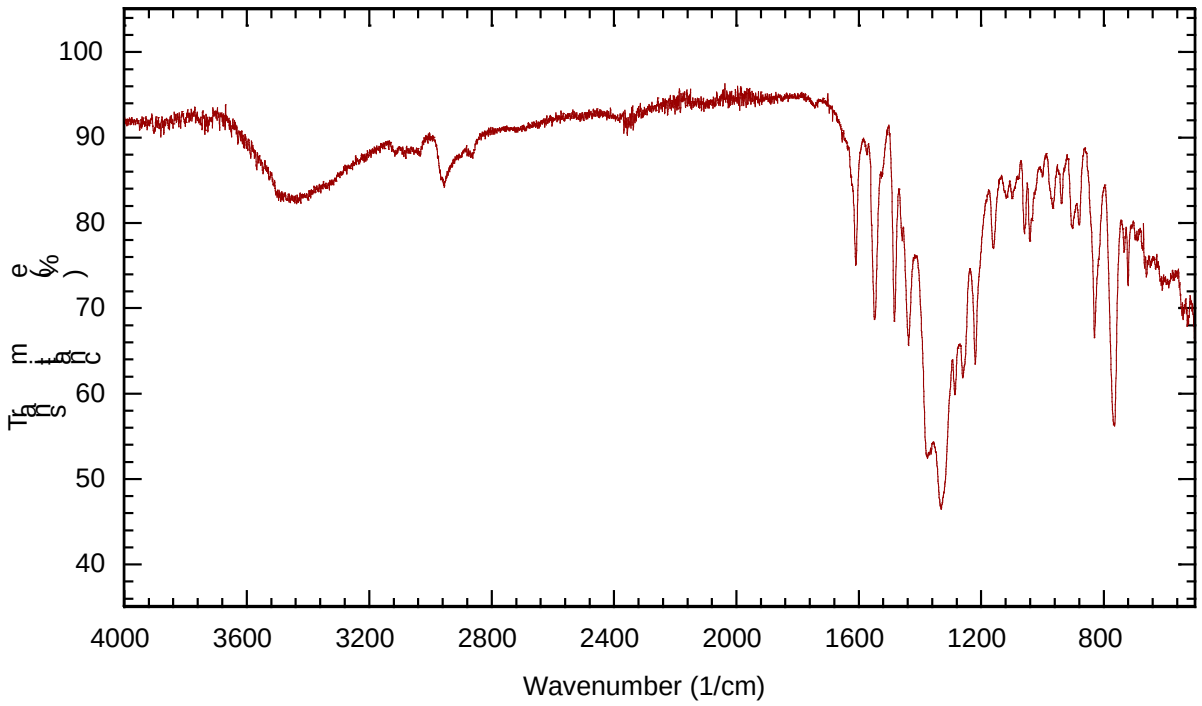

Figure S15. FT-IR Spectra of $[\{Co_2(bpbp)(O_2)\}_2(NH_2bdc)](NO_3)_4$.

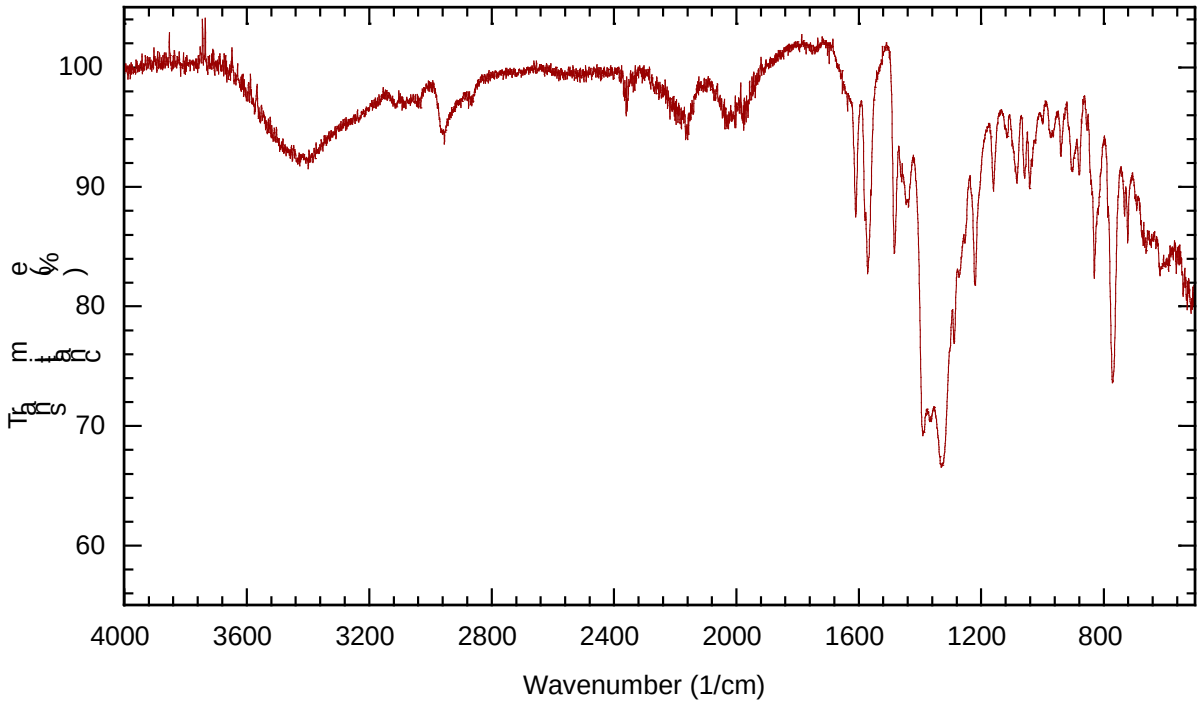

Figure S16. FT-IR Spectra of $[\{Co_2(bpbp)(O_2)\}_2(Cl_2bdc)](NO_3)_4$.

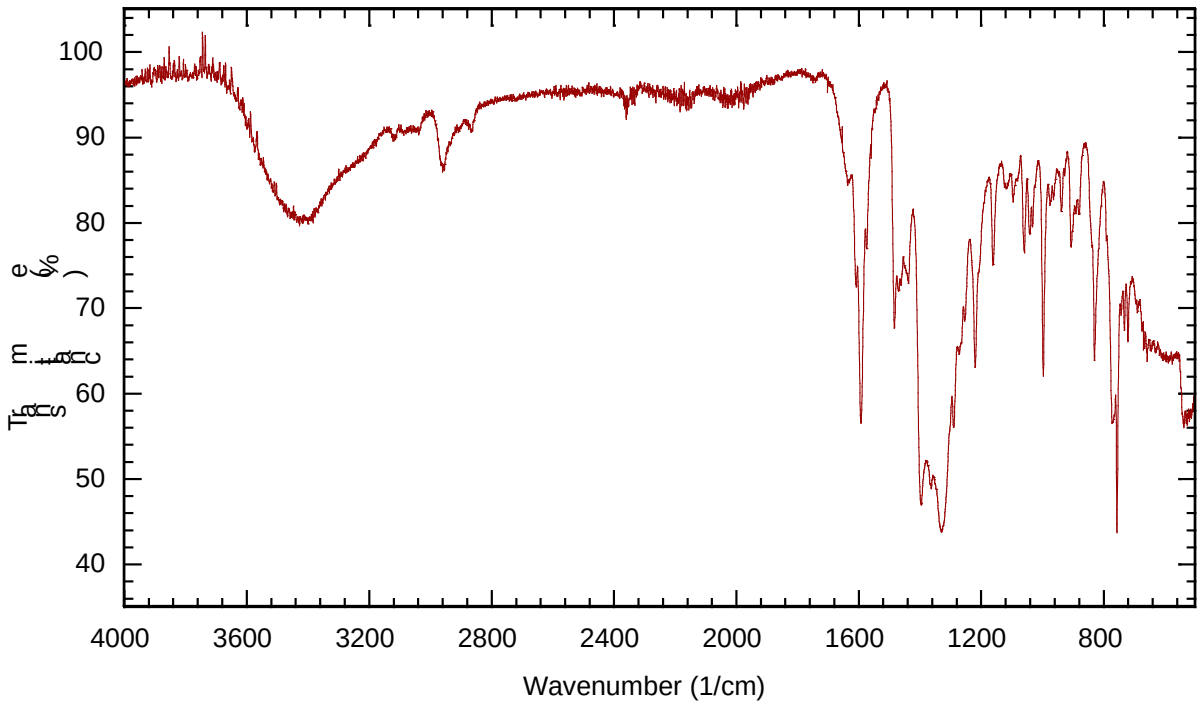

Figure S17. FT-IR Spectra of [{Co_2(bpbp)(O_2)}$_2$(F_4bdc)](NO_3)$_4$.